AIMS Mathematics, 11(4): 9066–9092.
DOI: 10.3934/math.2026374
Received: 18 January 2026
Revised: 24 March 2026
Accepted: 26 March 2026
Published: 02 April 2026

https://www.aimspress.com/journal/Math

Research article

Bifurcation analysis and solitary waves in a stochastic FitzHugh-Nagumo model

Jianping Zheng[1], Muhammad Abuzar[2], Luai Abdulla Aldoghan[3] and Mohammed Ahmed Alomair[3,*]

[1] College of Information Engineering, Hefei University of Economics, Hefei 230011, PR China

[2] School of Mathematical Sciences, Guizhou Normal University, Guiyang, Yunyan 550003, PR China

[3] Department of Quantitative Methods, School of Business, King Faisal University, Al-Ahsa 31982, Saudi Arabia

* **Correspondence:** Email: ma.alomair@kfu.edu.sa.

Abstract: The stochastic FitzHugh-Nagumo (FHN) equation is a fundamental model for excitable media, widely used to describe neuronal signal transmission and population dynamics under random perturbations. However, analytical studies that simultaneously incorporate stochastic effects, nonlinear wave propagation, and bifurcation behavior are still limited. In this work, we investigated a stochastic FHN model with multiplicative Gaussian noise and developed a unified analytical framework by integrating the unified method with a novel auxiliary equation technique. Using a stochastic transformation and expectation operator, the governing stochastic partial differential equation was reduced to a deterministic traveling-wave ordinary differential equation. This framework enables the systematic derivation of multiple classes of exact solutions, including rational, trigonometric, and hyperbolic soliton structures such as kink, anti-kink, periodic, and singular waves. Compared with existing methods, the proposed approach provides a more general mechanism for constructing diverse solution families within a single analytical structure. Furthermore, the reduced equation was reformulated into a planar dynamical system via a Galilean transformation, allowing bifurcation and phase-portrait analysis. Graphical results clearly illustrate the influence of noise intensity on wave morphology and temporal dynamics. The findings provide new analytical insights into noise-modulated excitation phenomena in stochastic nonlinear systems.

Keywords: stochastic model; analytical methods; solitary waves; bifurcation analysis; soliton solutions
Mathematics Subject Classification: 35C08, 37K40

1. Introduction

Nonlinear partial differential equations (NLPDEs) play a fundamental role in modeling complex spatio-temporal phenomena across physical, biological, and engineering systems [1, 2]. They provide a rigorous framework for analyzing wave propagation, pattern formation, and bifurcation behavior in nonlinear environments [3,4]. Among such models, the FHN equation is a widely studied prototype for excitable systems [5–7]. As a simplified representation of the Hodgkin-Huxley model [8], it captures key dynamical features such as threshold behavior, refractory effects, and traveling wave propagation, making it highly suitable for investigating nonlinear wave structures and dynamical transitions [9, 10]. Consequently, the FHN model serves as an important framework for studying excitation waves and bifurcation mechanisms in nonlinear systems [11].

The analysis of exact solutions, particularly soliton solutions, is essential for understanding nonlinear evolution equations [12, 13]. Solitons represent localized, stable waveforms arising from a balance between nonlinearity and dispersion/diffusion [14, 15]. To construct such solutions, numerous analytical techniques have been developed, including Lie symmetry analysis [16], the generalized Khater technique [17], the new auxiliary equation method (NAEM) [18, 19], the modified tanh method [20], the Kudryashov method [21], the Hirota method [22], the exponential rational function method [23], and the unified method (UM) [24, 25]. However, these approaches often produce limited solution families or rely on restrictive ansätz structures.

In realistic systems, deterministic models are insufficient due to unavoidable randomness. This motivates the study of stochastic PDEs, where noise is incorporated into the governing dynamics [26, 27]. Recent works have shown that stochastic effects significantly influence nonlinear wave behavior [28, 29]. In particular, multiplicative noise differs fundamentally from additive noise, as it is state-dependent and directly interacts with system dynamics [30], making it more suitable for modeling excitable systems such as the FHN equation. Despite these developments, analytical studies that simultaneously integrate stochastic effects, exact traveling-wave solutions, and bifurcation analysis for the FHN model remain limited [5, 7]. Existing approaches, such as Lie symmetry and generalized Khater methods, typically generate restricted solution classes or require strong assumptions. To address these limitations, this study develops a unified analytical framework for a stochastic FHN model with multiplicative Gaussian noise. Using a stochastic transformation and expectation operator, the model is reduced to a deterministic traveling-wave equation. The solution is then constructed using a combination of the UM [31, 32] and a novel auxiliary equation technique [33, 34].

Compared with existing methods, the proposed approach provides a systematic framework for generating multiple categories of solutions—including rational, trigonometric, and hyperbolic waveforms—within a single structure. Unlike Lie symmetry methods, it does not rely on invariant reductions, and compared to generalized Khater techniques, it avoids restrictive ansätz assumptions. Furthermore, the traveling-wave equation is analyzed using a bifurcation and phase-portrait framework, which reveals the stability and dynamical transitions of the obtained solutions [35–37]. This establishes a direct connection between exact solutions and phase-space dynamics.

Recent studies have explored various analytical techniques for nonlinear wave equations, including Kudryashov-based and fractional methods applied to systems such as the Fokas and nonlinear Schrödinger equations [38]. However, these works mainly focus on deterministic settings. In contrast,

the present study incorporates stochastic effects into the FHN model and extends unified analytical methods to noise-driven nonlinear systems [39]. The main contributions of this work are as follows. First, a stochastic FHN model with multiplicative Gaussian noise is analyzed via a mean-field traveling-wave reduction. Second, a unified analytical framework is developed to derive multiple classes of exact soliton solutions. Third, bifurcation and phase-portrait analysis are performed to explain the existence and stability of these solutions. Finally, the study provides new insight into noise-modulated nonlinear wave dynamics in excitable media.

The remainder of this paper is organized as follows. Section 2 presents the methodology. Section 3 introduces the stochastic FHN model. Section 4 derives exact solutions. Section 5 presents graphical analysis. Section 6 discusses bifurcation behavior. Section 7 concludes the paper.

2. Algorithm of analytical techniques

This section outlines the analytical framework employed to construct exact traveling-wave solutions of the proposed nonlinear model. The adopted techniques are designed to systematically reduce the governing partial differential equation into an ordinary differential equation and to generate closed-form solutions under suitable parametric constraints. In particular, the UM provides a flexible and efficient approach for deriving polynomial and rational solutions through the use of auxiliary equations and homogeneous balance principles. The essential steps and assumptions of this method are presented in detail below.

2.1. Unified method

Consider a general nonlinear partial differential equation of the form

$$G\left(x, t, g, \frac{\partial g}{\partial x}, \frac{\partial g}{\partial t}, \frac{\partial^2 g}{\partial x \partial t}, \frac{\partial^2 g}{\partial x^2}, \ldots\right) = 0, \tag{2.1}$$

where $g = g(x, t)$ denotes the dependent variable and $G(\cdot)$ represents a nonlinear functional involving g and its partial derivatives with respect to the independent variables x and t. The subscripts in G indicate partial derivatives with respect to the corresponding variables.

To construct exact traveling-wave solutions, we introduce the wave transformation

$$\eta = ux + vt,$$

where u and v are nonzero real constants representing the wave velocity parameters. Under this transformation, Eq (2.1) is reduced to an ordinary differential equation with respect to the single variable η, namely,

$$G\left(g, \frac{dg}{d\eta}, \frac{d^2 g}{d\eta^2}, \ldots\right) = 0. \tag{2.2}$$

This reduction transforms the original nonlinear PDE into a nonlinear ODE, which serves as the basis for constructing analytical wave solutions.

2.1.1. Polynomial solution

To derive polynomial-type solutions of Eq (2.2), we assume that the solution can be expressed in the form

$$g(\eta) = \sum_{k=0}^{N} r_k \varphi^k(\eta), \tag{2.3}$$

where r_k ($k = 0, 1, \ldots, N$) are unknown constants to be determined, and $\varphi(\eta)$ satisfies the auxiliary differential equation

$$(\varphi'(\eta))^{\alpha} = \sum_{k=0}^{\rho n} m_k \varphi^k(\eta), \qquad \rho = 1, 2, \tag{2.4}$$

with m_k being arbitrary constants and $\alpha \in \{1, 2\}$. The integer N is determined by applying the homogeneous balance principle between the highest-order derivative term and the nonlinear term appearing in Eq (2.2).

Substituting Eqs (2.3) and (2.4) into Eq (2.2) yields a polynomial equation in powers of $\varphi(\eta)$. By equating the coefficients of like powers to zero, a system of algebraic equations is obtained. Solving this system provides explicit expressions for the unknown parameters r_k and m_k, thereby yielding exact polynomial solutions of the original nonlinear PDE.

Notably, the UM admits solutions corresponding to $\alpha = 1$ and $\alpha = 2$, which lead to elementary and elliptic function solutions, respectively.

2.1.2. Rational solution

To derive rational-type solutions, we assume the following form:

$$g(\eta) = \frac{\sum_{i=0}^{N} r_i \varphi^i(\eta)}{\sum_{i=0}^{j} s_i \varphi^i(\eta)}, \tag{2.5}$$

where r_i and s_i are unknown constants, and $\varphi(\eta)$ satisfies the auxiliary equation

$$(\varphi'(\eta))^{\alpha} = \sum_{i=0}^{\rho k} b_i \varphi^i(\eta), \qquad \rho = 1, 2, \tag{2.6}$$

with b_i being arbitrary parameters and $\alpha \in \{1, 2\}$. The integers N and j are determined using the homogeneous balance principle by comparing the highest-order linear derivative term with the dominant nonlinear terms in Eq (2.2).

Substituting Eqs (2.5) and (2.6) into Eq (2.2) produces a rational expression in $\varphi(\eta)$. Applying the consistency criterion and equating the coefficients of like powers of $\varphi(\eta)$ in the resulting expression yields a system of algebraic equations. Solving this system determines the unknown coefficients r_i, s_i, and b_i, leading to explicit rational solutions of the governing nonlinear PDE.

Similar to the polynomial case, the UM allows the construction of both elementary ($\alpha = 1$) and elliptic ($\alpha = 2$) rational solutions, depending on the form of the auxiliary equation.

2.2. New auxiliary equation method

Although various analytical techniques are available for solving nonlinear fractional partial differential equations, many of them fail to adequately capture the combined effects of nonlinearity and damping. To overcome these limitations, we employ the NAEM, which provides a systematic framework for constructing exact analytical solitary wave solutions.

Consider a general nonlinear fractional partial differential equation of the form

$$P(F, F_x, F_t, F_{xx}, FF_t, \dots) = 0, \tag{2.7}$$

where $P(\cdot)$ is a nonlinear operator. By introducing a suitable traveling wave transformation, the above equation is reduced to a nonlinear ordinary differential equation (ODE)

$$R(\phi, \phi', \phi'', \phi\phi'', \dots) = 0, \tag{2.8}$$

where the prime denotes differentiation with respect to the traveling variable η, and $R(\cdot)$ consists of both linear and nonlinear terms.

According to the NAEM, the solution of Eq (2.8) is assumed in the form

$$\phi(\eta) = \sum_{i=0}^{N} f_i Q^{if(\eta)}, \tag{2.9}$$

where f_i $(i = 0, 1, 2, \dots, N)$ are constants to be determined, with $f_N \neq 0$. The auxiliary function $f(\eta)$ satisfies the differential equation

$$f'(\eta) = \frac{1}{\ln(Q)}\left(\varrho Q^{-f(\eta)} + \Omega + \mu Q^{f(\eta)}\right), \tag{2.10}$$

where ϱ, Ω, μ, and Q are real parameters.

The positive integer N is determined using the homogeneous balance principle by equating the highest-order derivative term with the dominant nonlinear term in Eq (2.8). Substituting Eq (2.9) into Eq (2.8) and collecting like powers of $Q^{f(\eta)}$ yield a system of nonlinear algebraic equations. Solving this system determines the unknown constants f_i, ϱ, Ω, and μ, leading to explicit analytical solutions.

Depending on the parametric constraints imposed on ϱ, Ω, and μ, the auxiliary equation admits multiple functional forms. Consequently, a wide variety of exact wave structures can be obtained. The admissible solution families are summarized below.

Family 1. For $\mu \neq 0$ and $\Omega^2 - 4\varrho\mu < 0$,

$$Q^{f(\eta)} = \frac{-\Omega}{2\mu} + \frac{\sqrt{4\varrho\mu - \Omega^2}}{2\mu}\tan\left(\frac{\sqrt{4\varrho\mu - \Omega^2}}{2}\eta\right), \tag{2.11}$$

$$Q^{f(\eta)} = \frac{-\Omega}{2\mu} - \frac{\sqrt{4\varrho\mu - \Omega^2}}{2\mu}\cot\left(\frac{\sqrt{4\varrho\mu - \Omega^2}}{2}\eta\right). \tag{2.12}$$

Family 2. When $\Omega^2 - 4\varrho\mu > 0$ and $\mu \neq 0$,

$$Q^{f(\eta)} = \frac{-\Omega}{2\mu} - \frac{\sqrt{\Omega^2 - 4\varrho\mu}}{2\mu} \tanh\left(\frac{\sqrt{\Omega^2 - 4\varrho\mu}}{2}\eta\right), \tag{2.13}$$

$$Q^{f(\eta)} = \frac{-\Omega}{2\mu} - \frac{\sqrt{\Omega^2 - 4\varrho\mu}}{2\mu} \coth\left(\frac{\sqrt{\Omega^2 - 4\varrho\mu}}{2}\eta\right). \tag{2.14}$$

Family 3. When $\Omega^2 + 4\varrho^2 < 0$ and $\mu = -\varrho$,

$$Q^{f(\eta)} = \frac{\Omega}{2\varrho} - \frac{\sqrt{-4\varrho^2 - \Omega^2}}{2\varrho} \tan\left(\frac{\sqrt{-4\varrho^2 - \Omega^2}}{2}\eta\right), \tag{2.15}$$

$$Q^{f(\eta)} = \frac{\Omega}{2\varrho} + \frac{\sqrt{-4\varrho^2 - \Omega^2}}{2\varrho} \cot\left(\frac{\sqrt{-4\varrho^2 - \Omega^2}}{2}\eta\right). \tag{2.16}$$

The remaining families (Families 4–20) correspond to special parametric choices of ϱ, Ω, and μ, yielding hyperbolic, trigonometric, rational, and exponential wave structures. These solution classes collectively demonstrate the versatility of the NAEM in capturing diverse nonlinear wave phenomena, including solitary waves, periodic waves, singular solutions, and rational profiles.

Family 4. When $\Omega^2 + 4\varrho^2 > 0$, $\mu \neq 0$, and $\mu = -\varrho$,

$$Q^{f(\eta)} = \frac{\Omega}{2\varrho} + \frac{\sqrt{4\varrho^2 + \Omega^2}}{2\varrho} \tanh\left(\frac{\sqrt{4\varrho^2 + \Omega^2}}{2}\eta\right), \tag{2.17}$$

$$Q^{f(\eta)} = \frac{\Omega}{2\varrho} + \frac{\sqrt{4\varrho^2 + \Omega^2}}{2\varrho} \coth\left(\frac{\sqrt{4\varrho^2 + \Omega^2}}{2}\eta\right). \tag{2.18}$$

Family 5. When $\Omega^2 - 4\varrho^2 < 0$ and $\mu = \varrho$,

$$Q^{f(\eta)} = \frac{-\Omega}{2\varrho} + \frac{\sqrt{4\varrho^2 - \Omega^2}}{2\varrho} \tan\left(\frac{\sqrt{4\varrho^2 - \Omega^2}}{2}\eta\right), \tag{2.19}$$

$$Q^{f(\eta)} = \frac{-\Omega}{2\varrho} - \frac{\sqrt{4\varrho^2 - \Omega^2}}{2\varrho} \cot\left(\frac{\sqrt{4\varrho^2 - \Omega^2}}{2}\eta\right). \tag{2.20}$$

Family 6. When $\Omega^2 - 4\varrho^2 > 0$ and $\mu = \varrho$,

$$Q^{f(\eta)} = \frac{-\Omega}{2\varrho} - \frac{\sqrt{-4\varrho^2 + \Omega^2}}{2\varrho} \tanh \frac{\sqrt{-4\varrho^2 + \Omega^2}}{2}\eta\Big), \tag{2.21}$$

$$Q^{f(\eta)} = \frac{-\Omega}{2\varrho} - \frac{\sqrt{-4\varrho^2 + \Omega^2}}{2\varrho} \coth\left(\frac{\sqrt{-4\varrho^2 + \Omega^2}}{2}\eta\right). \tag{2.22}$$

Family 7. When $\Omega^2 = 4\varrho\mu$,

$$Q^{f(\eta)} = -\frac{2 + \Omega\eta}{2\mu\eta}. \tag{2.23}$$

Family 8. For $\varrho\mu < 0$, $\Omega = 0$ and $\mu \neq 0$,

$$Q^{f(\eta)} = -\sqrt{\frac{-\varrho}{\mu}}\tanh(\sqrt{-\varrho\mu}\eta), \tag{2.24}$$

$$Q^{f(\eta)} = -\sqrt{-\frac{\varrho}{\mu}}\coth(\sqrt{-\varrho\mu}\eta). \tag{2.25}$$

Family 9. Where $\varrho = -\mu$ with $\Omega = 0$,

$$Q^{f(\eta)} = -\left(\frac{e^{-2\mu\eta}+1}{1-e^{-2\mu\eta}}\right). \tag{2.26}$$

Family 10. Where $\varrho = \mu = 0$,

$$Q^{f(\eta)} = \sinh(\Omega\eta) + \cosh(\Omega\eta). \tag{2.27}$$

Family 11. Where $\varrho = \Omega = c$ and $\mu = 0$,

$$Q^{f(\eta)} = e^{c\eta} - 1. \tag{2.28}$$

Family 12. Where $\mu = \Omega = c$ and $\varrho = 0$,

$$Q^{f(\eta)} = \frac{e^{c\eta}}{1-e^{c\eta}}. \tag{2.29}$$

Family 13. Where $\Omega = \varrho + \mu$,

$$Q^{f(\eta)} = -\frac{1-\varrho e^{(\varrho-\mu)\eta}}{1-\mu e^{(\varrho-\mu)\eta}}. \tag{2.30}$$

Family 14. Where $\Omega = -\mu - \varrho$,

$$Q^{f(\eta)} = \frac{e^{(-\mu+\varrho)\eta}-\varrho}{e^{(\varrho-\mu)\eta}-\mu}. \tag{2.31}$$

Family 15. Where $\varrho = 0$,

$$Q^{f(\eta)} = \frac{\Omega e^{\Omega\eta}}{1-\mu e^{\Omega\eta}}. \tag{2.32}$$

Family 16. Where $\varrho = \Omega = \mu \neq 0$,

$$Q^{f(\eta)} = \frac{1}{2}\left[\sqrt{3}\tan(\frac{\sqrt{3}}{2}\varrho\eta) - 1\right]. \tag{2.33}$$

Family 17. Where $\Omega = \mu = 0$,

$$Q^{f(\eta)} = \varrho\eta. \tag{2.34}$$

Family 18. Where $\Omega = \varrho = 0$,

$$Q^{f(\eta)} = -\frac{1}{\mu\eta}. \tag{2.35}$$

Family 19. Where $\mu = \varrho$ and $\Omega = 0$,

$$Q^{f(\eta)} = \tan(\varrho\eta). \tag{2.36}$$

Family 20. Where $\mu = 0$,

$$Q^{f(\eta)} = e^{\Omega\eta} - \frac{j}{l}. \tag{2.37}$$

3. Governing model

This section presents the mathematical formulation of the stochastic FHN model considered in this study. The model is employed to describe the evolution of excitable systems in the presence of random perturbations, capturing the combined effects of diffusion, nonlinear reaction kinetics, and stochastic excitation. Such formulations are widely used to investigate wave propagation, pattern formation, and stability properties in biological and physical systems subject to environmental or intrinsic noise. The governing equation and its associated assumptions are introduced below [5, 7]:

$$F_t = dF_{xx} + F(F - a)(1 - F) + \sigma F\,\dot{W}(t), \tag{3.1}$$

where $F = F(x, t)$ denotes the state variable. In physical and biological contexts, F represents the state variable describing excitation dynamics as well as the dynamical behavior of nerve impulse transmission in neural systems. The parameter a satisfies $0 < a < 1$, $d > 0$ is the diffusion coefficient, $W(t)$ denotes a standard Wiener process, $\dot{W}(t) = \frac{dW(t)}{dt}$ represents Gaussian white noise in time, and σ is the noise intensity parameter.

To construct traveling-wave solutions of Eq (3.1), we introduce the stochastic transformation

$$F(x, t) = \phi(\eta)\exp\left(\sigma W(t) - \frac{\sigma^2}{2}t\right), \quad \eta = ux + vt, \tag{3.2}$$

where η is the traveling wave variable, where u is the wave number, v is the wave velocity, and $\phi(\eta)$ is a deterministic wave profile to be determined. Substituting transformation (3.2) into Eq (3.1) yields

$$-v\phi' + u^2 d\phi'' + \phi\left(\phi e^{\sigma W(t) - \frac{\sigma^2}{2}t} - a\right)\left(1 - \phi e^{\sigma W(t) - \frac{\sigma^2}{2}t}\right) = 0, \tag{3.3}$$

where the prime denotes differentiation with respect to η.

Taking the mathematical expectation of Eq (3.3) and using the well-known identity for the Wiener process,

$$\mathbb{E}\left(e^{\sigma W(t)}\right) = e^{\frac{\sigma^2}{2}t},$$

the stochastic exponential terms are eliminated. Consequently, the governing stochastic partial differential equation is reduced to the deterministic nonlinear ordinary differential equation

$$-v\phi' + u^2 d\phi'' + \phi(\phi - a)(1 - \phi) = 0. \tag{3.4}$$

Equation (3.4) serves as the fundamental traveling-wave equation associated with the stochastic FHN model and forms the basis for constructing exact analytical solutions using the proposed analytical techniques. It should be emphasized that Eq (3.4) represents the expected (mean-field) dynamics of the stochastic FHN model. Although the original system Eq (3.1) contains multiplicative noise, the application of the expectation operator removes the explicit stochastic term due to the properties of the Wiener process. Consequently, the reduced traveling-wave equation does not explicitly depend on the noise intensity parameter σ. Therefore, the subsequent analytical results describe the averaged behavior of the stochastic system rather than its full stochastic dynamics.

For $\sigma \neq 0$, prior to taking the expectation, the transformed equation contains stochastic exponential terms and can be interpreted as a random differential equation. However, after applying the expectation operator, these stochastic contributions vanish, leading to the deterministic Eq (3.4). As a result, the influence of noise is not directly reflected in the analytical form of the reduced equation, but manifests through statistical and qualitative effects on wave dynamics. The present model incorporates multiplicative noise of the form $\sigma F\dot{W}(t)$, which differs fundamentally from additive noise. In multiplicative noise, the stochastic perturbation depends on the system state, leading to amplitude-dependent fluctuations and stronger interaction with the nonlinear reaction terms. This results in enhanced sensitivity of wave solutions, particularly near steep gradients or singular structures. In contrast, additive noise introduces uniform perturbations that do not directly couple with the system state and typically have a weaker influence on the qualitative structure of traveling waves. Therefore, multiplicative noise plays a more significant role in modulating wave propagation and stability in excitable systems.

4. Soliton solutions

4.1. Application of the unified method

The rational function solution and the polynomial function solution are the two ways in which we obtain the solutions to the governing model using the UM.

4.1.1. Polynomial function solutions

Assume the initial form of solution is as follows:

$$\phi(\eta) = \sum_{k=0}^{N} r_k \varphi^k(\eta), \tag{4.1}$$

$$(\varphi\prime(\eta))^{\alpha} = \sum_{k=0}^{\rho n} m_k \varphi^k(\eta), \quad \rho = 1, 2, \tag{4.2}$$

where r_k are unknown coefficients and m_k are arbitrary constants of the auxiliary equation. We now get $N = 1$ by applying the homogeneous balancing principle between the dispersive and nonlinear factors. We create a relationship between N and n such that $N = n - 1$ for any $k > 2$ by applying the balancing principle. We address two examples for the polynomial function solution: $k = 1$, $\rho = 1$, and $k = 1$,

$\rho = 2$. Equation (4.1) is reduced to

$$\phi(\eta) = \sum_{k=0}^{1} r_k \varphi^k(\eta), \tag{4.3}$$

$$(\varphi\prime(\eta))^{1\rho} = \sum_{k=0}^{\rho n} m_k \varphi^k(\eta), \quad \rho = 1, 2. \tag{4.4}$$

Variables r_k and m_k will be found later.

Case 1.

Considering $\rho = 1$ and $n = 1$ in Eqs (4.3) and (4.4), Eq (4.3) becomes

$$\phi(\eta) = r_0 + r_1 \varphi(\eta), \tag{4.5}$$

$$\varphi'(\eta) = m_0 + m_1 \varphi(\eta) + m_2 \varphi^2(\eta). \tag{4.6}$$

First, the auxiliary Eq (4.6) is substituted in Eq (4.5). Then by substituting the assumed solution, which is consistent with the auxiliary equation, into Eq (3.4), a system of algebraic equations is obtained as shown below.

$$\begin{aligned}
&20d\,u^2 m_2^2 r_1 - r_1^3 = 0,\\
&3d\,u^2 m_1 m_2 r_1 + a r_1^2 - v m_2 r_1 - 3 r_0 r_1^2 + r_1^2 = 0,\\
&2d\,u^2 m_0 m_2 r_1 + d\,u^2 m_1^2 r_1 + 2a r_0 r_1 - v m_1 r_1 - 3 r_0^2 r_1 - a r_1 + 2 r_0 r_1 = 0,\\
&u^2 d r_1 m_1 m_0 + r_0^2 a - v r_1 m_0 - r_0^3 - r_0 a + r_0^2 = 0.
\end{aligned}$$

The resulting algebraic system is solved with the help of Maple software, and the following results are obtained:

$$v = \frac{\sqrt{2}\,\sqrt{d}u\,(a+1)}{2}, \quad m_0 = \frac{\left(-2du^2 m_1^2 + a^2 - 2a + 1\right)\sqrt{2}}{8u\sqrt{d} r_1}, \quad m_1 = m_1, \tag{4.7}$$

$$m_2 = -\frac{r_1\sqrt{2}}{2\sqrt{d}u}, \quad r_0 = -\frac{m_1\sqrt{2}\,\sqrt{d}u}{2} + \frac{a}{2} + \frac{1}{2}, \quad r_1 = r_1. \tag{4.8}$$

Equations (4.7) and (4.8) are integrated into the governing model's ODE to produce the following result.

$$F_1(x,t) = \left(\frac{a + \tanh\left(\frac{\eta\sqrt{2}(a-1)}{4u\sqrt{d}}\right)(a-1) + 1}{2} \right) e^{\sigma W - \frac{\sigma^2}{2}}. \tag{4.9}$$

Case 2.

Here, taking $\rho = 2$ and $k = 1$ in Eqs (4.3) and (4.4), then Eq (4.3) will have the following form:

$$\phi(\eta) = r_0 + r_1 \varphi(\eta), \tag{4.10}$$

$$\varphi'(\eta) = \varphi(\eta)\sqrt{m_0 + m_1\varphi(\eta) + m_2\varphi^2(\eta)}. \tag{4.11}$$

First, Eq (4.5) has been substituted in the auxiliary Eq (4.6). A system of algebraic equations is obtained as follows by inserting the assumed solution, which is consistent with the auxiliary equation, into Eq (3.4):

$$\begin{aligned}
&4d^2u^4m_2^2r_1^2 - 4d\,u^2m_2r_1^4 + r_1^6 = 0,\\
&6d^2u^4m_1m_2r_1^2 + 4ad\,u^2m_2r_1^3 - 3d\,u^2m_1r_1^4 - 12d\,u^2m_2r_0r_1^3 + 4d\,u^2m_2r_1^3 - 2ar_1^5 + 6r_0r_1^5 - 2r_1^5 = 0,\\
&-9u^2dr_1^3m_1r_0 + 3u^2dr_1^3m_1a + 4u^4d^2r_1^2m_2m_0 + r_1^4a^2 + 15r_0^2r_1^4 - 10r_0r_1^4 + 4r_1^4a + 8u^2dr_1^2m_2r_0a\\
&-2u^2dr_1^4m_0 + \frac{9}{4}u^4d^2r_1^2m_1^2 + 3u^2dr_1^3m_1 + r_1^4 - 12u^2dr_1^2m_2r_0^2 + 8u^2dr_1^2m_2r_0 - 4u^2dr_1^2m_2a\\
&-v^2r_1^2m_2 - 10r_0r_1^4a = 0,\\
&3u^4d^2r_1^2m_0m_1 + 2u^2dr_1^3m_0a + 6u^2dr_1^2m_1r_0a + 4u^2dr_1m_2r_0^2a - 6u^2dr_1^3m_0r_0\\
&-9u^2dr_1^2m_1r_0^2 - 4u^2dr_1m_2r_0^3 - 3u^2dr_1^2m_1a - 4u^2dr_1m_2r_0a + 2u^2dr_1^3m_0 + 6u^2dr_1^2m_1r_0\\
&+4u^2dr_1m_2r_0^2 + 4r_0a^2r_1^3 - 20r_0^2r_1^3a + 20r_0^3r_1^3 - 2r_1^3a^2 + 16r_0r_1^3a - v^2r_1^2m_1 - 20r_0^2r_1^3 - 2r_1^3a + 4r_0r_1^3 = 0,\\
&u^4d^2r_1^2m_0^2 + 4u^2dr_1^2m_0r_0a + 3u^2dr_1m_1r_0^2a - 6u^2dr_1^2m_0r_0^2 - 3u^2dr_1m_1r_0^3 - 2u^2dr_1^2m_0a - 3u^2dr_1m_1r_0a\\
&+4u^2dr_1^2m_0r_0 + 3u^2dr_1m_1r_0^2 + 6r_0^2a^2r_1^2 - 20r_0^3r_1^2a + 15r_0^4r_1^2 - 6r_0a^2r_1^2 + 24r_0^2r_1^2a - v^2r_1^2m_0 - 20r_0^3r_1^2 + r_1^2a^2\\
&-6r_0r_1^2a + 6r_0^2r_1^2 = 0,\\
&2u^2dr_1m_0r_0^2a - 2u^2dr_1m_0r_0^3 - 2u^2dr_1m_0r_0a + 2u^2dr_1m_0r_0^2 + 4r_0^3a^2r_1 - 10r_0^4ar_1 + 6r_0^5r_1 - 6r_0^2a^2r_1\\
&+16r_0^3ar_1 - 10r_0^4r_1 + 2r_0a^2r_1 - 6r_0^2r_1a + 4r_0^3r_1 = 0,\\
&r_0^4a^2 - 2r_0^5a + r_0^6 - 2r_0^3a^2 + 4r_0^4a - 2r_0^5 + r_0^2a^2 - 2r_0^3a + r_0^4 = 0.
\end{aligned}$$

Employing computer tools to solve the system of equations for the unknown values, we can get the subsequent parameters:

$$v = \frac{\sqrt{2}\sqrt{d}\,(a+1)\,u}{2}, \quad m_0 = \frac{(a-1)^2}{2u^2d}, \quad m_2 = \frac{du^2m_1^2}{2(a-1)^2}, \quad r_0 = 1, \quad r_1 = -\frac{du^2m_1}{a-1} \tag{4.12}$$

and the following result is obtained by applying Eq (4.12) to Eq (4.10).

$$F_2(x,t) = \left(\frac{2\mathrm{e}^{\frac{\eta\sqrt{2}\sqrt{\frac{(a-1)^2}{u^2d}}}{2}}m_1a - 1}{2\mathrm{e}^{\frac{\eta\sqrt{2}\sqrt{\frac{(a-1)^2}{u^2d}}}{2}}m_1 - 1}\right)e^{\sigma W - \frac{\sigma^2}{2}}. \tag{4.13}$$

4.1.2. Rational function solution

Assume that the initial solution takes the following rational form:

$$\phi(\eta) = \frac{\sum_{k=0}^{N} r_k\varphi^k(\eta)}{\sum_{k=0}^{R} s_k\varphi^k(\eta)}, \tag{4.14}$$

$$(\varphi'(\eta))^\rho = \sum_{k=0}^{\rho n} b_k\varphi^k(\eta), \quad \rho = 1, 2. \tag{4.15}$$

Here, r_k, s_k, and b_k are unknown constants appearing in Eqs (4.14) and (4.15). These constants are determined by applying the consistency criterion. By employing the homogeneous balance principle, the relationship $N - R = n - 1$ is obtained. In this work, we focus exclusively on the case where $N = R$ with $\rho = 2$. Consequently, the assumed forms reduce to

$$\phi(\eta) = \frac{r_0 + r_1\varphi(\eta)}{s_0 + s_1\varphi(\eta)} \tag{4.16}$$

and

$$\varphi'(\eta) = \sqrt{b_0 + b_1\varphi(\eta) + b_2\varphi^2(\eta)}. \tag{4.17}$$

By substituting the assumed solution into the auxiliary equation in (3.1), we obtain the algebraic system. The unknown coefficients are determined by solving the resulting algebraic system. This procedure yields the following parameter values:

$$v = \frac{\sqrt{2}\,\sqrt{d}(a-2)u}{2}, \quad b_0 = \frac{s_0^2}{8du^2s_1^2}, \quad b_1 = \frac{as_0}{2du^2s_1}, \quad b_2 = \frac{a^2}{2u^2d}, \quad r_0 = \frac{s_0}{2}, \quad r_1 = as_1. \tag{4.18}$$

Accordingly, the rational traveling-wave solution of the governing model is expressed as

$$F_3(x,t) = \left(\frac{\mathrm{e}^{\frac{\eta\sqrt{2}a}{2u\sqrt{d}}} as_1 u\sqrt{d}}{\sqrt{d}\mathrm{e}^{\frac{\eta\sqrt{2}a}{2u\sqrt{d}}} us_1 + s_0\sqrt{2}\left(a - \frac{1}{2}\right)} \right) \mathrm{e}^{\sigma W - \frac{\sigma^2}{2}}. \tag{4.19}$$

4.2. New auxiliary equation method

This subsection is devoted to the construction of exact analytical solutions for the governing model using the new auxiliary equation method. By applying the homogeneous balance principle to Eq (3.4), the balancing number is obtained as $N = 1$. Consequently, the assumed solution in Eq (2.9) can be rewritten in the form

$$\phi(\eta) = f_0 + f_1 Q^{f(\eta)}. \tag{4.20}$$

Substituting Eq (4.20) into Eq (3.4), together with the auxiliary Eq (2.10), and equating the coefficients of identical powers of $Q^{f(\eta)}$ to zero yields the following system of algebraic equations:

$$\begin{aligned}
&(Q^{f(\eta)})^0 : \ \Omega d\varrho u^2 f_1 + af_0^2 - vf_1\varrho - f_0^3 - af_0 + f_0^2 = 0,\\
&(Q^{f(\eta)})^1 : \ \Omega^2 du^2 f_1 + 2d\mu\varrho u^2 f_1 - \Omega v f_1 + 2af_0 f_1 - 3f_0^2 f_1 - af_1 + 2f_0 f_1 = 0,\\
&(Q^{f(\eta)})^2 : \ 3\Omega d\mu u^2 f_1 + af_1^2 - \mu v f_1 - 3f_0 f_1^2 + f_1^2 = 0,\\
&(Q^{f(\eta)})^3 : \ 2d\mu^2 u^2 f_1 - f_1^3 = 0.
\end{aligned}$$

By solving the above algebraic system with the aid of Maple software, the following parameter values are obtained:

$$f_0 = \frac{\Omega}{2}\sqrt{\frac{1}{\Omega^2 - 4\varrho\mu}} + \frac{1}{2}, \quad f_1 = \mu\sqrt{\frac{1}{\Omega^2 - 4\varrho\mu}}, \quad a = \frac{\sqrt{\frac{1}{\Omega^2-4\varrho\mu}} + 2v}{2\sqrt{\frac{1}{\Omega^2-4\varrho\mu}}}, \quad d = \frac{1}{2\left(\Omega^2 - 4\varrho\mu\right)u^2}. \tag{4.21}$$

Accordingly, Eq (4.20) is reduced to

$$\phi(\eta) = \frac{1}{2} + \frac{\left(2\mu\, Q^{f(\eta)} + \Omega\right)\sqrt{\frac{1}{\Omega^2-4\varrho\mu}}}{2}. \tag{4.22}$$

By substituting the explicit forms of $Q^{f(\eta)}$ given in Eqs (2.11)–(2.37) into Eq (4.22), a variety of exact surface wave solutions can be constructed. These solutions are classified into several families according to the parametric constraints. The first family is presented below.

Family 1. For $\mu \neq 0$ and $\Omega^2 - 4\varrho\mu < 0$, the solutions take the form

$$F_4(x,t) = \left(\frac{1}{2} + \frac{\sqrt{-\Omega^2+4\varrho\mu}\,\tan\left(\frac{\sqrt{-\Omega^2+4\varrho\mu}\,\eta}{2}\right)\sqrt{\frac{1}{\Omega^2-4\varrho\mu}}}{2}\right)e^{\sigma W-\frac{\sigma^2}{2}}, \tag{4.23}$$

$$F_5(x,t) = \left(\frac{1}{2} - \frac{\sqrt{-\Omega^2+4\varrho\mu}\,\cot\left(\frac{\sqrt{-\Omega^2+4\varrho\mu}\,\eta}{2}\right)\sqrt{\frac{1}{\Omega^2-4\varrho\mu}}}{2}\right)e^{\sigma W-\frac{\sigma^2}{2}}. \tag{4.24}$$

Family 2. When $\Omega^2 - 4\varrho\mu > 0$ and $\mu \neq 0$:

$$F_6(x,t) = \left(\frac{1}{2} - \frac{\sqrt{\Omega^2-4\varrho\mu}\,\tanh\left(\frac{\sqrt{\Omega^2-4\varrho\mu}\,\eta}{2}\right)\sqrt{\frac{1}{\Omega^2-4\varrho\mu}}}{2}\right)e^{\sigma W-\frac{\sigma^2}{2}}, \tag{4.25}$$

$$F_7(x,t) = \left(\frac{1}{2} - \frac{\sqrt{\Omega^2-4\varrho\mu}\,\coth\left(\frac{\sqrt{\Omega^2-4\varrho\mu}\,\eta}{2}\right)\sqrt{\frac{1}{\Omega^2-4\varrho\mu}}}{2}\right)e^{\sigma W-\frac{\sigma^2}{2}}. \tag{4.26}$$

Family 3. When $\Omega^2 + 4\varrho^2 < 0$, $\mu \neq 0$, and $\mu = -\varrho$:

$$F_8(x,t) = \left(\frac{-\sqrt{\frac{1}{\Omega^2-4\varrho\mu}}\,\sqrt{-\Omega^2-4\varrho^2}\,\tan\left(\frac{\sqrt{-\Omega^2-4\varrho^2}\,\eta}{2}\right)\mu + \Omega\,(\mu+\varrho)\,\sqrt{\frac{1}{\Omega^2-4\varrho\mu}} + \varrho}{2\varrho}\right)e^{\sigma W-\frac{\sigma^2}{2}}, \tag{4.27}$$

$$F_9(x,t) = \left(\frac{\cot\left(\frac{\sqrt{-\Omega^2-4\varrho^2}\,\eta}{2}\right)\sqrt{\frac{1}{\Omega^2-4\varrho\mu}}\,\sqrt{-\Omega^2-4\varrho^2}\,\mu + \Omega\,(\mu+\varrho)\,\sqrt{\frac{1}{\Omega^2-4\varrho\mu}} + \varrho}{2\varrho}\right)e^{\sigma W-\frac{\sigma^2}{2}}. \tag{4.28}$$

Family 4. When $\Omega^2 + 4\varrho^2 > 0$, $\mu \neq 0$, and $\mu = -\varrho$:

$$F_{10}(x,t) = \left(\frac{\sqrt{\frac{1}{\Omega^2-4\varrho\mu}}\,\tanh\left(\frac{\sqrt{\Omega^2+4\varrho^2}\,\eta}{2}\right)\sqrt{\Omega^2+4\varrho^2}\,\mu + \Omega\,(\mu+\varrho)\,\sqrt{\frac{1}{\Omega^2-4\varrho\mu}} + \varrho}{2\varrho}\right)e^{\sigma W-\frac{\sigma^2}{2}}, \tag{4.29}$$

$$F_{11}(x,t) = \left(\frac{\sqrt{\frac{1}{\Omega^2-4\varrho\mu}}\,\coth\left(\frac{\sqrt{\Omega^2+4\varrho^2}\,\eta}{2}\right)\sqrt{\Omega^2+4\varrho^2}\,\mu + \Omega\,(\mu+\varrho)\,\sqrt{\frac{1}{\Omega^2-4\varrho\mu}} + \varrho}{2\varrho}\right)e^{\sigma W-\frac{\sigma^2}{2}}. \tag{4.30}$$

Family 5. When $\Omega^2 - 4\varrho^2 < 0$ and $\mu = \varrho$:

$$F_{12}(x,t) = \left(\frac{\sqrt{\frac{1}{\Omega^2-4\varrho\mu}}\, \tan\left(\frac{\sqrt{-\Omega^2+4\varrho^2}\,\eta}{2} \right) \sqrt{-\Omega^2+4\varrho^2}\,\mu - \Omega\,(\mu-\varrho)\, \sqrt{\frac{1}{\Omega^2-4\varrho\mu}} + \varrho}{2\varrho} \right) e^{\sigma W - \frac{\sigma^2}{2}}, \tag{4.31}$$

$$F_{13}(x,t) = \left(\frac{-\sqrt{\frac{1}{\Omega^2-4\varrho\mu}}\, \cot\left(\frac{\sqrt{-\Omega^2+4\varrho^2}\,\eta}{2} \right) \sqrt{-\Omega^2+4\varrho^2}\,\mu - \Omega\,(\mu-\varrho)\, \sqrt{\frac{1}{\Omega^2-4\varrho\mu}} + \varrho}{2\varrho} \right) e^{\sigma W - \frac{\sigma^2}{2}}. \tag{4.32}$$

Family 6. When $\Omega^2 - 4\varrho^2 > 0$ and $\mu = \varrho$:

$$F_{14}(x,t) = \left(\frac{-\sqrt{\Omega^2-4\varrho^2}\, \tanh\left(\frac{\sqrt{\Omega^2-4\varrho^2}\,\eta}{2} \right) \sqrt{\frac{1}{\Omega^2-4\varrho\mu}}\,\mu - \Omega\,(\mu-\varrho)\, \sqrt{\frac{1}{\Omega^2-4\varrho\mu}} + \varrho}{2\varrho} \right) e^{\sigma W - \frac{\sigma^2}{2}}, \tag{4.33}$$

$$F_{15}(x,t) = \left(\frac{-\sqrt{\Omega^2-4\varrho^2}\, \coth\left(\frac{\sqrt{\Omega^2-4\varrho^2}\,\eta}{2} \right) \sqrt{\frac{1}{\Omega^2-4\varrho\mu}}\,\mu - \Omega\,(\mu-\varrho)\, \sqrt{\frac{1}{\Omega^2-4\varrho\mu}} + \varrho}{2\varrho} \right) e^{\sigma W - \frac{\sigma^2}{2}}. \tag{4.34}$$

Family 7. When $\Omega^2 = 4\varrho\mu$:

$$F_{16}(x,t) = \frac{\eta - 2\sqrt{\frac{1}{\Omega^2-4\varrho\mu}}}{2\eta}. \tag{4.35}$$

Family 8. For $\varrho\mu < 0$, $\Omega = 0$, and $\mu \neq 0$:

$$F_{17}(x,t) = \left(\frac{1}{2} + \frac{\left(-2\sqrt{-\frac{\varrho}{\mu}}\, \tanh\left(\sqrt{-\varrho\mu}\,\eta \right) \mu + \Omega \right) \sqrt{\frac{1}{\Omega^2-4\varrho\mu}}}{2} \right) e^{\sigma W - \frac{\sigma^2}{2}}, \tag{4.36}$$

$$F_{18}(x,t) = \left(\frac{1}{2} + \frac{\left(-2\sqrt{-\frac{\varrho}{\mu}}\, \coth\left(\sqrt{-\varrho\mu}\,\eta \right) \mu + \Omega \right) \sqrt{\frac{1}{\Omega^2-4\varrho\mu}}}{2} \right) e^{\sigma W - \frac{\sigma^2}{2}}. \tag{4.37}$$

Family 9. When $\varrho = -\mu$ with $\Omega = 0$:

$$F_{19}(x,t) = \left(\frac{(1 + \operatorname{csgn}\left(\frac{1}{\mu}\right)) e^{-2\mu\eta} + (\operatorname{csgn}\left(\frac{1}{\mu}\right) - 1)}{2(e^{-2\mu\eta} - 1)} \right) e^{\sigma W - \frac{\sigma^2}{2}}. \tag{4.38}$$

Family 12. When $\mu = \Omega = c$ and $\varrho = 0$:

$$F_{20}(x,t) = \left(\frac{(-\mathrm{e}^{c\eta} - 1) \operatorname{csgn}\left(\frac{1}{c}\right) - 1 + \mathrm{e}^{c\eta}}{-2 + 2\mathrm{e}^{c\eta}} \right) e^{\sigma W - \frac{\sigma^2}{2}}. \tag{4.39}$$

Family 13. When $\Omega = \varrho + \mu$,

$$F_{21}(x,t) = \left(\frac{\mu \left(\operatorname{csgn}\left(\frac{1}{\mu-\varrho}\right) + 1 \right) e^{-(\mu-\varrho)\eta} + \left(\operatorname{csgn}\left(\frac{1}{\mu-\varrho}\right) - 1 \right)}{2\left(\mu e^{-(\mu-\varrho)\eta} - 1\right)} \right) e^{\sigma W - \frac{\sigma^2}{2}}. \tag{4.40}$$

Family 14. When $\Omega = -\mu - \varrho$:

$$F_{22}(x,t) = \left(\frac{\mathrm{e}^{-(\mu-\varrho)\eta} \operatorname{csgn}\left(\frac{1}{\mu-\varrho}\right) + \operatorname{csgn}\left(\frac{1}{\mu-\varrho}\right)\mu + \mathrm{e}^{-(\mu-\varrho)\eta} - \mu}{2\mathrm{e}^{-(\mu-\varrho)\eta} - 2\mu} \right) e^{\sigma W - \frac{\sigma^2}{2}}. \tag{4.41}$$

Family 15. When $\varrho = 0$:

$$F_{23}(x,t) = \left(\frac{-\mathrm{e}^{\Omega\eta} \operatorname{csgn}\left(\frac{1}{\Omega}\right)\mu + \mu \mathrm{e}^{\Omega\eta} - \operatorname{csgn}\left(\frac{1}{\Omega}\right) - 1}{2\mu \mathrm{e}^{\Omega\eta} - 2} \right) e^{\sigma W - \frac{\sigma^2}{2}}. \tag{4.42}$$

Family 16. When $\varrho = \Omega = \mu \neq 0$:

$$F_{24}(x,t) = \left(\frac{-\mathrm{e}^{\Omega\eta} \operatorname{csgn}\left(\frac{1}{\Omega}\right)\mu + \mu \mathrm{e}^{\Omega\eta} - \operatorname{csgn}\left(\frac{1}{\Omega}\right) - 1}{2\mu \mathrm{e}^{\Omega\eta} - 2} \right) e^{\sigma W - \frac{\sigma^2}{2}}. \tag{4.43}$$

Family 19. For $\mu = \varrho =$ and $\Omega = 0$:

$$F_{25}(x,t) = \left(\frac{1}{2} + \frac{\tan(\eta\varrho)\,\varrho \sqrt{-\frac{1}{\varrho^2}}}{2} \right) e^{\sigma W - \frac{\sigma^2}{2}}. \tag{4.44}$$

5. Graphical discussion of the results

The graphical representations presented in this section serve to validate the derived analytical traveling-wave solutions derived for the stochastic FHN equation and to illustrate the influence of multiplicative noise on their qualitative behavior. The exact solutions admit clear physical interpretations. Kink-type and anti-kink waveforms correspond to transitions between distinct stable equilibrium states of the system and are characteristic of excitable dynamics. In neuronal modeling, such waves represent the initiation and recovery phases of action potentials, during which the membrane potential rapidly switches between resting and excited states. Periodic solutions, on the other hand, arise from closed orbits around center-type equilibria in the reduced phase plane and are associated with oscillatory excitation regimes, such as rhythmic neural firing. Rational and singular solutions describe sharp-fronted or highly localized excitation events driven by strong nonlinear interactions.

Figures 1 and 2 illustrate the impact of the noise intensity (σ) on the wave morphology, where all physical quantities are expressed in arbitrary units (a.u.). In this analytical context, the solution at $\sigma = 0$ represents the mean (deterministic) behavior, while the deviations observed at higher σ values represent the variance introduced by the multiplicative Gaussian noise. Despite these fluctuations, the

topological structure of the waves remains structurally intact, demonstrating the structural stability of the FHN system under random perturbations.

Specifically, Figure 1 illustrates the rational function solution $F_3(x,t)$ for the parameter values $a = 0.8$, $s_1 = u = 1$, $d = 0.5$, and $s_0 = 2$. The three-dimensional surface plot in Figure 1(a) demonstrates a coherent traveling-wave structure that propagates steadily along the spatial direction. The corresponding two-dimensional profiles shown in Figure 1(b) confirm the monotonic transition between equilibrium states. The stochastic influence on the solution is further examined through sample path plots in Figure 1(c)–(f). For low noise intensities, the stochastic trajectories remain tightly clustered around the deterministic solution, indicating robustness. As the noise intensity σ increases (e.g., from 0.3 to 0.9), temporal fluctuations and intermittent spikes become more pronounced, reflecting noise-induced modulation of the excitation amplitude. Despite this increased variability, the overall wave profile and decay behavior are preserved, highlighting the stabilizing role of the underlying nonlinear dynamics.

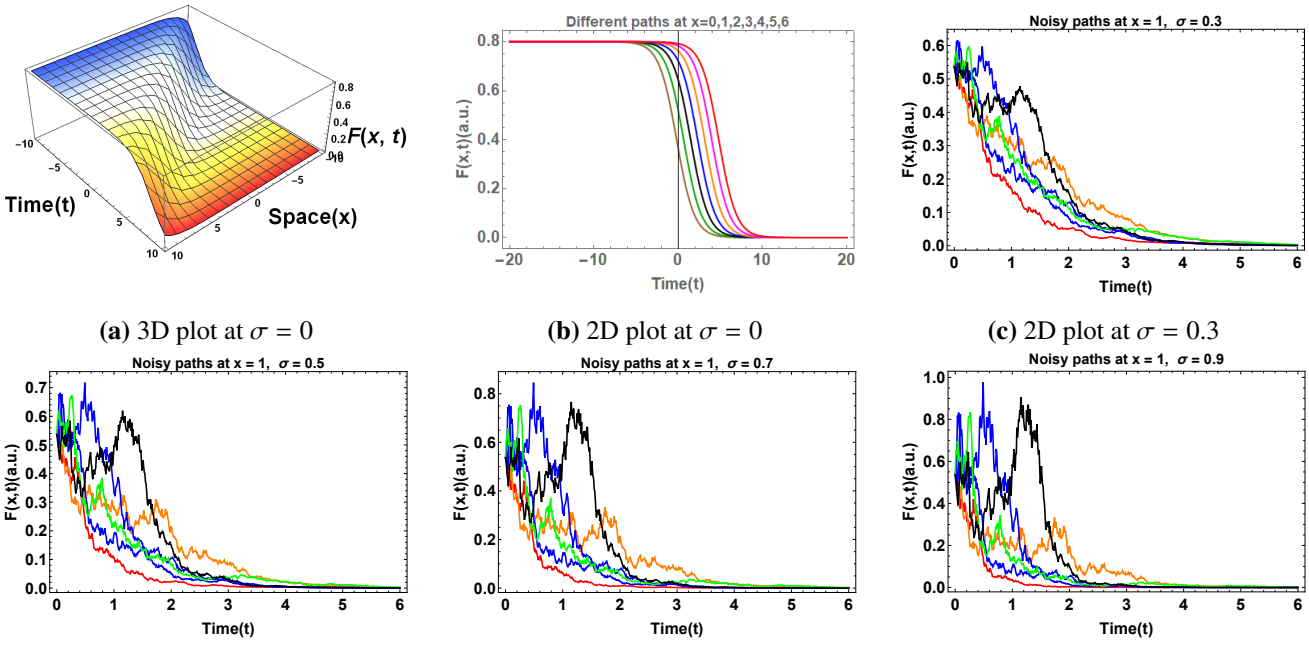

(a) 3D plot at $\sigma = 0$ **(b)** 2D plot at $\sigma = 0$ **(c)** 2D plot at $\sigma = 0.3$

(d) 2D plot at $\sigma = 0.5$ **(e)** 2D plot at $\sigma = 0.7$ **(f)** 2D plot at $\sigma = 0.9$

Figure 1. Graphical representation of the rational solution $F_3(x,t)$ of the stochastic FHN equation for $a = 0.8$, $s_1 = u = 1$, $d = 0.5$, and $s_0 = 2$. (a) Three-dimensional surface plot showing the spatio-temporal evolution of a coherent traveling wave. (b) Two-dimensional temporal profiles indicating a kink-type transition between equilibrium states. (c)–(f) Sample stochastic trajectories at $x = 1$ for increasing noise intensities $\sigma = 0.3$, 0.5, 0.7, and 0.9, respectively, illustrating noise-induced amplitude fluctuations while preserving the global wave structure.

Figure 2 illustrates the dynamical behavior of the rational solution $F_{18}(x,t)$ for the parameter set $\varrho = -3$, $\mu = 2$, $u = 1$, and $v = -0.5$. The 3D surface plot in Figure 2(a) exhibits a pronounced singular wave structure defined by steep spatial gradients and rapid temporal transitions. Correspondingly,

the 2D profiles in Figure 2(b) confirm the existence of sharp excitation fronts, which are indicative of the strong nonlinearities inherent in rational-type analytical structures. To evaluate the statistical response of this singular waveform, Figure 2(c)–(f) depict the stochastic trajectories under varying noise intensities σ, where all axes are calibrated in arbitrary units (a.u.).

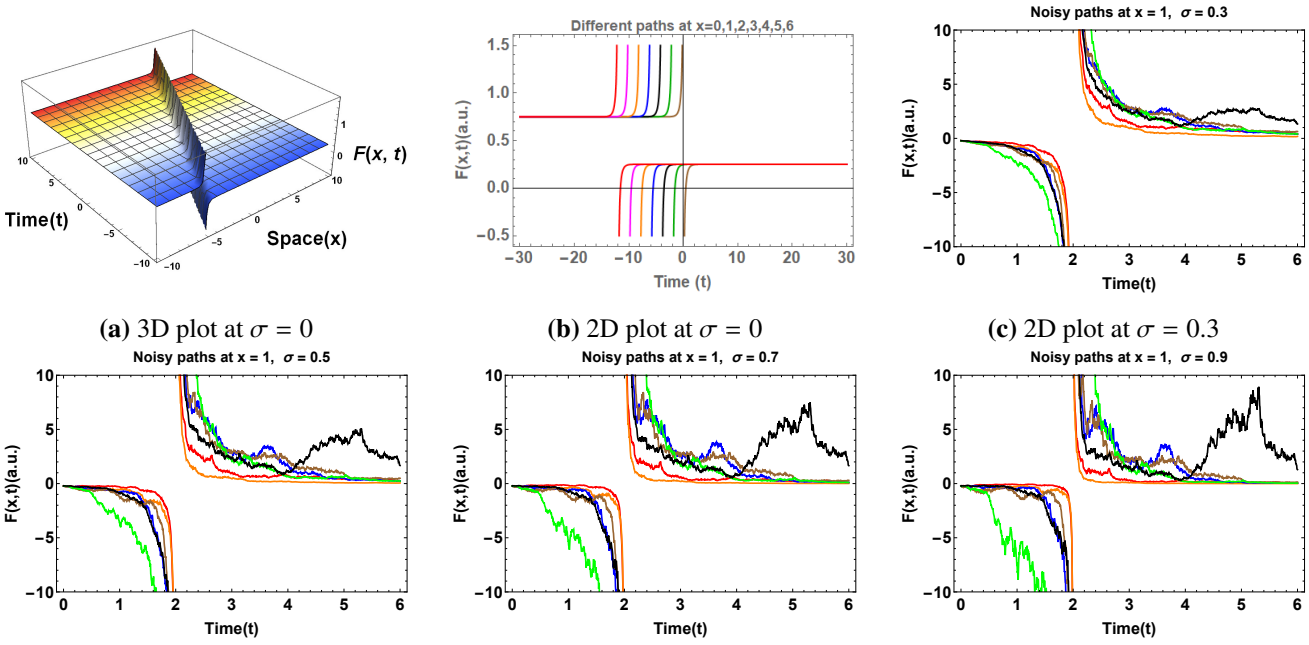

(a) 3D plot at $\sigma = 0$ **(b)** 2D plot at $\sigma = 0$ **(c)** 2D plot at $\sigma = 0.3$

(d) 2D plot at $\sigma = 0.5$ **(e)** 2D plot at $\sigma = 0.7$ **(f)** 2D plot at $\sigma = 0.9$

Figure 2. Graphical illustration of the rational solution $F_{18}(x,t)$ for $\varrho = -3$, $\mu = 2$, $u = 1$, and $v = -0.5$. (a) Three-dimensional surface plot revealing a singular wave structure with sharp spatial gradients. (b) Two-dimensional temporal profiles highlighting abrupt transitions driven by strong nonlinearity. (c)–(f) Stochastic trajectories at $x = 1$ for increasing noise intensities $\sigma = 0.3$, 0.5, 0.7, and 0.9, showing enhanced sensitivity of the singular waveform to stochastic perturbations.

Compared to the smoother kink-type solution $F_3(x,t)$, the trajectories of $F_{18}(x,t)$ display significantly higher sensitivity to noise, particularly in regions of high gradients. As the noise intensity σ increases, the variance of the fluctuations grows, leading to increasingly asymmetric and irregular paths. In this context, the analytical solution represents the mean state of the system, while the deviations observed in the sample paths illustrate the stochastic modulation of the excitation amplitude. Despite this variability, the global wave structure remains identifiable, suggesting that multiplicative noise primarily drives local amplitude fluctuations without collapsing the fundamental wave pattern.

From a physical perspective, these results provide critical insights into excitable dynamics under random influences. In neurophysics, while kink and anti-kink solutions model the initiation and termination of action potentials, singular and rational waveforms represent abrupt excitation bursts triggered by intrinsic or external fluctuations. In the context of reaction-diffusion systems, these solutions describe the propagation of invasion fronts in heterogeneous environments, where stochastic modulation captures environmental uncertainty and disturbance rejection. This graphical analysis

confirms that while increasing σ enhances temporal irregularity and amplitude variance, the underlying nonlinear dynamics of the stochastic FHN equation maintain the robustness of the traveling-wave structures. This complex interplay between noise and nonlinearity underscores the necessity of stochastic modeling for a high-fidelity description of real-world excitable systems.

The observed fluctuations in the graphical results further confirm that multiplicative noise primarily affects the amplitude and local stability of wave solutions without completely altering their global structure. This indicates that while the deterministic bifurcation framework captures the underlying phase-space geometry, stochastic effects introduce variability around these deterministic trajectories.

6. Bifurcation analysis

It should be emphasized that the bifurcation analysis presented in this section is based on the deterministic mean-field system obtained after expectation. In the original stochastic system, multiplicative noise can introduce fluctuations around equilibrium points and may shift bifurcation thresholds in a probabilistic sense. In particular, near critical parameter regimes, stochastic perturbations can induce transitions between different dynamical states, thereby affecting the stability and persistence of traveling-wave solutions.

Traveling-wave solutions of nonlinear reaction-diffusion equations can be studied effectively through phase-plane analysis. Under the traveling-wave transformation, the stochastic FHN equation reduces to a planar dynamical system whose trajectories correspond to different classes of wave solutions. In particular, solitary waves arise from homoclinic or heteroclinic orbits, while periodic traveling waves correspond to closed orbits surrounding center-type equilibria. Therefore, bifurcation and phase portrait analysis provides a dynamical explanation for the existence and stability of the exact soliton solutions derived in Section 4. In this section, we investigate the qualitative dynamical behavior of the traveling-wave solutions of the stochastic FHN model by means of bifurcation theory and phase portrait analysis. To derive the planar dynamical system, we first introduce the Galilean (traveling wave) transformation

$$\eta = x - vt, \quad \phi(x,t) = \phi(\eta),$$

where v is the wave speed. Under this transformation, the derivatives become

$$\phi_t = -v\phi', \quad \phi_x = \phi', \quad \phi_{xx} = \phi'',$$

where the prime denotes differentiation with respect to η. Substituting these into (3.4), we obtain the ordinary differential equation

$$-v\phi' + u^2 d\phi'' + \phi(\phi - a)(1 - \phi) = 0.$$

Next, by introducing $P = \dfrac{d\phi}{d\eta}$, the above second-order equation can be rewritten as the following planar dynamical system:

$$\begin{cases} \frac{d\phi}{d\eta} = P, \\ \frac{dP}{d\eta} = z_1\phi^3 + z_2\phi^2 + z_3\phi + z_4 P, \end{cases} \tag{6.1}$$

where

$$z_1 = \frac{1}{u^2 d}, \quad z_2 = \frac{a-1}{u^2 d}, \quad z_3 = \frac{a}{u^2 d}, \quad z_4 = \frac{v}{u^2 d}.$$

6.1. Equilibrium points and linear stability

The equilibrium points of system (6.1) are obtained by setting $P = 0$ and solving

$$z_1\phi^3 + z_2\phi^2 + z_3\phi = 0. \tag{6.2}$$

The qualitative behavior of system (6.1) is governed by the roots of the cubic polynomial

$$G(\phi) = z_1\phi^3 + z_2\phi^2 + z_3\phi,$$

whose discriminant determines the number of equilibrium points. When the discriminant is positive, three real equilibrium points coexist, whereas a negative discriminant yields a single equilibrium point. The transition between these regimes corresponds to a saddle-node bifurcation, marking a qualitative change in the traveling-wave dynamics and the admissible wave structures. Depending on the discriminant of the cubic polynomial in (6.2), the system admits either a single equilibrium point or three distinct equilibrium points. When the discriminant is negative, a unique equilibrium point exists at

$$U_1 = (0, 0).$$

For a positive discriminant, three equilibrium points arise:

$$U_1 = (0, 0), \quad U_2 = \left(\frac{-z_2 + \sqrt{z_2^2 - 4z_1z_3}}{2z_1}, 0 \right), \quad U_3 = \left(\frac{-z_2 - \sqrt{z_2^2 - 4z_1z_3}}{2z_1}, 0 \right).$$

To classify the stability of each equilibrium, system (6.1) is linearized about $(\phi_i, 0)$. The Jacobian matrix is given by

$$\mathbf{J}(\phi_i, 0) = \begin{pmatrix} 0 & 1 \\ G'(\phi_i) & z_4 \end{pmatrix}, \quad G(\phi) = z_1\phi^3 + z_2\phi^2 + z_3\phi.$$

The determinant of the Jacobian,

$$\det \mathbf{J}(\phi_i, 0) = -G'(\phi_i),$$

determines the nature of the equilibrium point: A negative determinant corresponds to a center, while a positive determinant indicates a saddle point.

6.2. Phase portrait analysis

To illustrate the different dynamical regimes predicted by the above analysis, ten representative phase portraits in the (ϕ, P)-plane are presented for distinct parameter configurations. Figure 3 displays a phase portrait corresponding to a parameter regime in which three equilibrium points exist. The middle equilibrium U_2 exhibits center-type behavior, while U_1 and U_3 are saddle points, forming separatrix trajectories that bound closed orbits.

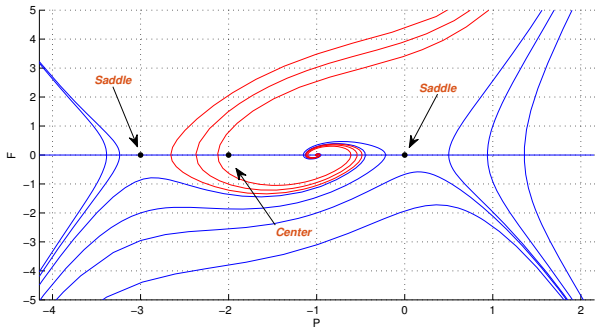

Figure 3. Phase portrait of system (6.1) with three equilibrium points, where the central equilibrium is a center and the remaining equilibria are saddles.

Figure 4 shows another configuration with three equilibrium points, illustrating a similar saddle-center-saddle structure but with modified separatrix geometry due to parameter variation.

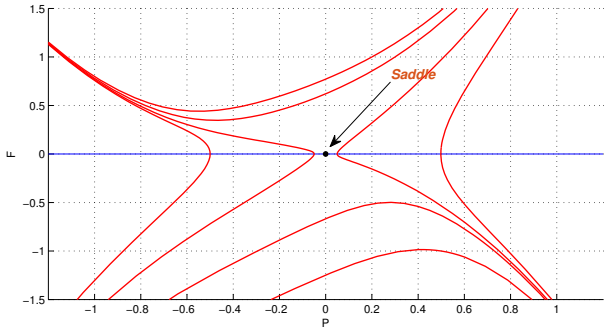

Figure 4. Phase portrait corresponding to a three-equilibrium configuration with altered separatrix structure.

Figure 5 presents a phase portrait for a parameter set in which the system admits only a single equilibrium point. The trajectories indicate saddle-type behavior, implying instability of the associated traveling-wave solution.

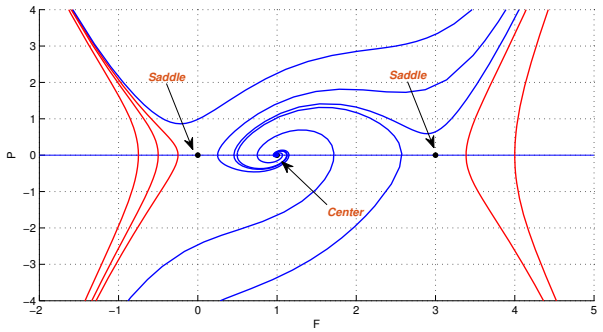

Figure 5. Phase portrait corresponding to a single equilibrium point exhibiting saddle behavior.

A similar single-equilibrium configuration is shown in Figure 6, confirming the robustness of saddle-type dynamics under different parameter choices.

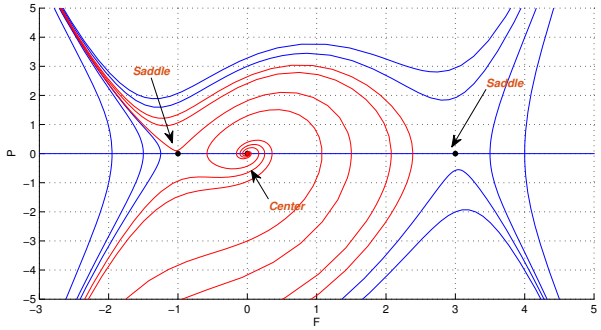

Figure 6. Phase portrait illustrating saddle-type dynamics for a single equilibrium point under a different parameter regime.

Figures 7 and 8 demonstrate bifurcation scenarios in which equilibrium points merge as the discriminant approaches zero. These phase portraits indicate the onset of qualitative changes in the system's dynamical structure.

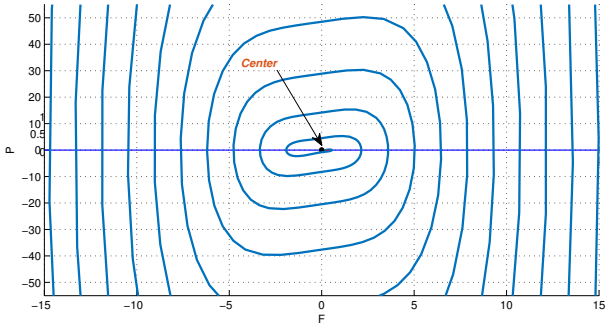

Figure 7. Phase portrait near a bifurcation threshold where equilibrium points coalesce.

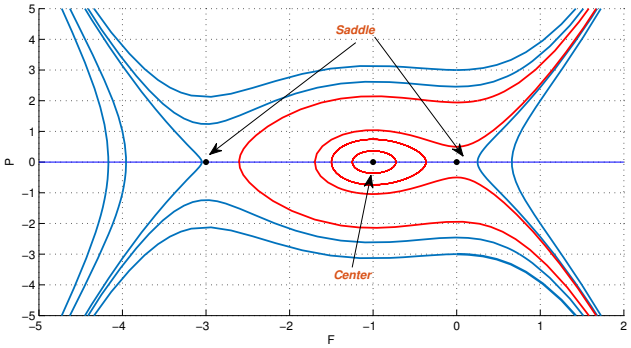

Figure 8. Phase portrait illustrating the transition between center and saddle configurations close to bifurcation.

Figures 9 and 10 present additional bifurcation-induced configurations, highlighting changes in stability and separatrix topology as control parameters vary.

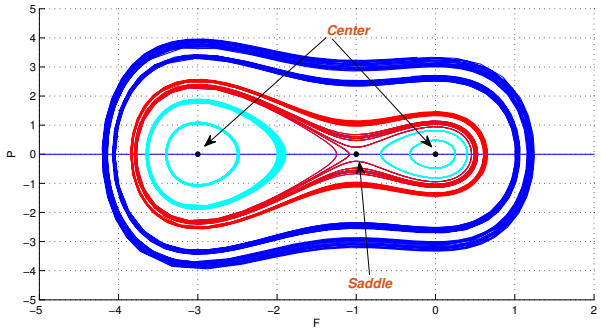

Figure 9. Phase portrait showing a change in stability of equilibrium points induced by parameter variation.

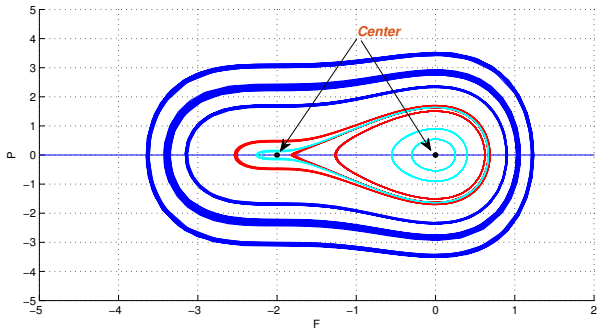

Figure 10. Phase portrait illustrating a degenerate bifurcation case with modified phase-space topology.

Finally, Figures 11 and 12 depict limiting or degenerate cases of the planar system, further confirming the sensitivity of the traveling-wave dynamics to parameter changes.

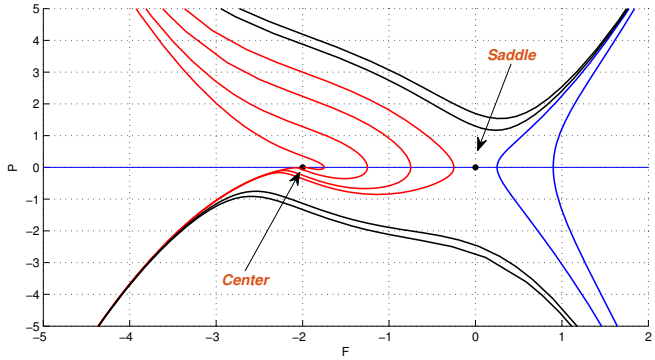

Figure 11. Phase portrait corresponding to a limiting parameter configuration of system (6.1).

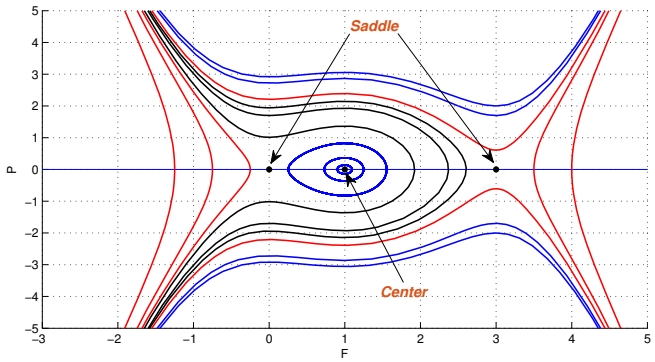

Figure 12. Phase portrait illustrating a degenerate equilibrium configuration in the (ϕ, P)-plane.

Overall, the phase portrait analysis demonstrates how variations in system parameters govern the number and stability of equilibrium points, thereby controlling the qualitative behavior of traveling-wave solutions. The observed saddle-center structures and bifurcation transitions provide a dynamical explanation for the existence and stability of the soliton solutions derived in the previous sections. In summary, the bifurcation and phase portrait analysis provides a rigorous dynamical foundation for the exact solutions obtained in this work. The observed saddle-center structures, homoclinic and heteroclinic connections, and bifurcation transitions explain how nonlinear traveling-wave solutions arise, persist, or disappear as system parameters vary. This analysis confirms that the stochastic FHN model exhibits rich wave dynamics consistent with excitable media theory.

7. Conclusions

In this paper, we have successfully investigated the bifurcation behavior and exact solitary wave solutions of the stochastic FitzHugh-Nagumo model under multiplicative Gaussian noise. By employing a unified analytical framework and a novel auxiliary equation technique, we derived diverse classes of solutions, including kink, anti-kink, periodic, and singular structures. While this work provides significant insights into the impact of noise on wave morphology, several avenues remain for extending the current research.

Despite the results obtained, this study is limited by the assumption of standard white Gaussian noise. Therefore, a primary direction for future work is studying the impact of non-Gaussian noise, such as Lévy stable noise or colored noise, on the stability and propagation of soliton solutions in the FHN model. Such an extension would better capture the heavy-tailed fluctuations often observed in complex biological systems.

Furthermore, the current model assumes instantaneous signal transmission. Real-world neuronal systems inherently involve signal propagation latencies [40]; hence, extending the analytical framework to the stochastic FHN model with a time delay represents a vital next step. This would allow for the investigation of how delay-induced bifurcations interact with stochastic perturbations to alter neural firing patterns.

Finally, while our analytical solutions provide a theoretical foundation, conducting experimental verification through high-fidelity numerical simulations or comparison with recorded

electrophysiological data is necessary. Bridging the gap between these exact mathematical profiles and empirical observations will further validate the applicability of the proposed stochastic FHN framework to actual excitable media.

Author contributions

All authors contributed equally to the preparation of this manuscript. All authors have read and approved the final version of the manuscript for publication.

Use of Generative-AI tools declaration

The authors declare they have not used Artificial Intelligence tools in the creation of this article.

Funding

This work was supported by the Deanship of Scientific Research, Vice Presidency for Graduate Studies and Scientific Research, King Faisal University, Saudi Arabia [Grant No. KFU261470].

Conflict of interest

All authors declare no conflicts of interest in this paper.

References

1. E. Mosekilde, O. G. Mouritsen, *Modelling the dynamics of biological systems: Nonlinear phenomena and pattern formation*, Berlin, Heidelberg: Springer. https://doi.org/10.1007/978-3-642-79290-8
2. U. Budag, E. Yaşar, Exact analytical solutions of the modified complex Ginzburg-Landau equation: Multi-waves, bright and dark solitons via systematic integration approaches, *Int.l J. Mod. Phys. B*, **40** (2026), 2650025. https://doi.org/10.1142/S0217979226500256
3. K. A. Abdul Al Woadud, D. Kumar, A. R. Khan, Local bifurcation behavior, chaos, and oblique travelling wave structures in the (2+1)-dimensional chiral Schrödinger equation with beta derivative, *Chaos Soliton. Fract.*, **204** (2026), 117726. https://doi.org/10.1016/j.chaos.2025.117726
4. R. Ur Rahman, Z. Li, J. He, Magnetic wave dynamics in ferromagnetic thin films: Interactions of solitons and positons in Landau-Lifshitz-Gilbert equation, *Physica D*, **479** (2025), 134719. https://doi.org/10.1016/j.physd.2025.134719
5. M. W. Yasin, M. S. Iqbal, N. Ahmed, A. Akgül, A. Raza, M. Rafiq, et al., Numerical scheme and stability analysis of stochastic Fitzhugh-Nagumo model, *Results Phys.*, **32** (2022), 105023. https://doi.org/10.1016/j.rinp.2021.105023
6. J. Fu, X. Y. Zhang, Q. Fang, A sixth-order compact finite difference framework for solving nonlinear reaction-diffusion equations: Application to FitzHugh-Nagumo model, *AIMS Mathematics*, **10** (2025), 21040–21060. https://doi.org/10.3934/math.2025940

7. M. S. Iqbal, M. Inc, M. W. Yasin, N. Ahmed, F. M. Tawfiq, M. Bilal, et al., Soliton solutions of nonlinear stochastic Fitz-Hugh Nagumo equation, *Opt. Quant. Electron.*, **56** (2024), 1047. https://doi.org/10.1007/s11082-024-06819-4
8. H. Wiese, E. Koppenhofer, On the capacity current in myelinated nerve fibres, *Gen. Physiol. Biophys.*, **2** (1983), 297–312.
9. D. Priyadarsini, P. K. Sahu, M. Routaray, A combined Taylor-Bernstein approximation for solving non-linear Fitz-Hugh-Nagumo equation, *Int. J. Appl. Comput. Math.*, **10** (2024), 110. https://doi.org/10.1007/s40819-024-01744-2
10. M. A. Elfouly, M. A. Sohaly, M. E. Fares, FitzHugh-Nagumo model in neutral delay differential equation representation, *Acta Biotheor.*, **74** (2026), 7. https://doi.org/10.1007/s10441-025-09513-4
11. H. Tian, X. Yi, Y. Zhang, Z. Wang, X. Xi, J. Liu, Dynamical analysis, feedback control circuit implementation, and fixed-time sliding mode synchronization of a novel 4D chaotic system, *Symmetry*, **17** (2025), 1252. https://doi.org/10.3390/sym17081252
12. S. Ahmad, N. Becheikh, L. Kolsi, T. Muhammad, Z. Ahmad, M. K. Nasrat, Uncovering the stochastic dynamics of solitons of the Chaffee-Infante equation, *Sci. Rep.*, **14** (2024), 19485. https://doi.org/10.1038/s41598-024-67116-4
13. M. M. Al-Sawalha, H. Yasmin, R. Shah, A. H. Ganie, K. Moaddy, Unraveling the dynamics of singular stochastic solitons in stochastic fractional Kuramoto-Sivashinsky equation, *Fractal Fract.*, **7** (2023), 753. https://doi.org/10.3390/fractalfract7100753
14. R. U. Rahman, Z. Li, J. He, Kink-type wavefronts in some saturated ferromagnetic materials Via the Darboux transformation, *Math. Method. Appl. Sci.*, **48** (2025), 8735–8754. https://doi.org/10.1002/mma.10750
15. S. Xu, J. He, Various rational solutions generated from the higher order Kaup–Newell type equation, *Chaos Soliton. Fract.*, **201** (2025), 117286. https://doi.org/10.1016/j.chaos.2025.117286
16. S. Kumar, S. Rani, N. Mann, Analytical soliton solutions to a (2+1)-dimensional variable coefficients graphene sheets equation using the application of Lie symmetry approach: Bifurcation theory, sensitivity analysis and chaotic behavior, *Qual. Theory Dyn. Syst.*, **24** (2025), 80. https://doi.org/10.1007/s12346-025-01232-y
17. T. Younas, J. Ahmad, Novel soliton insights into generalized fractional Tzitzéica-type evolution equations using the modified Khater method, *Mod. Phys. Lett. B*, **39** (2025), 2450441. https://doi.org/10.1142/S0217984924504414
18. N. Raza, A. Jhangeer, R. Ur Rahman, A. R. Butt, Y. M. Chu, Sensitive visualization of the fractional Wazwaz-Benjamin-Bona-Mahony equation with fractional derivatives: A comparative analysis, *Results Phys.*, **25** (2021), 104171. https://doi.org/10.1016/j.rinp.2021.104171
19. R. Ur Rahman, M. M. M. Qousini, A. Alshehri, S. M. Eldin, K. El-Rashidy, M. S. Osman, Evaluation of the performance of fractional evolution equations based on fractional operators and sensitivity assessment, *Results Phys.*, **49** (2023), 106537. https://doi.org/10.1016/j.rinp.2023.106537

20. A. Tarek, H. M. Ahmed, N. Badra, I. Samir, Soliton dynamics and stability in resonant nonlinear Schrödinger systems with cubic quintic effects via enhanced modified extended tanh function method, *Sci. Rep.*, **15** (2025), 42916. https://doi.org/10.1038/s41598-025-27692-5

21. S. T. R. Rizvi, S. O. Abbas, S. Ghafoor, A. Althobaiti, A. R. Seadawy, Soliton solutions with generalized Kudryashov method and study of variational integrators with Lagrangian to shallow water wave equation, *Mod. Phys. Lett. A*, **40** (2025), 2550043. https://doi.org/10.1142/S0217732325500439

22. M. Wang, G. He, T. Xu, Wronskian solutions and N-soliton solutions for the Hirota–Satsuma equation, *Appl. Math. Lett.*, **159** (2025), 109279. https://doi.org/10.1016/j.aml.2024.109279

23. B. Kopçasız, F. N. K. Sağlam, Exploration of soliton solutions for the Kaup–Newell model using two integration schemes in mathematical physics, *Math. Method. Appl. Sci.*, **48** (2025), 6477–6487. https://doi.org/10.1002/mma.10684

24. J. Ahmad, Z. Mustafa, M. Anwar, M. Kouki, N. A. Shah, Exploring solitonic wave dynamics in the context of nonlinear conformable Kairat-X equation via unified method, *AIMS Mathematics*, **10** (2025), 10898–10916. https://doi.org/10.3934/math.2025495

25. T. Aydemir, Comparative analysis of the generalized unified method with some exact solution methods and general solutions of the Biswas-Milovic equation, *Theor. Math. Phys.*, **222** (2025), 119–130. https://doi.org/10.1134/S004057792501009X

26. Y. A. Madani, S. Hussain, M. A. Almalahi, B. Muflh, K. A. Aldwoah, M. Y. Y. Abdalla, Comprehensive study of stochastic soliton solutions in nonlinear models with application to the Davey Stewartson equations, *Sci. Rep.*, **15** (2025), 18169. https://doi.org/10.1038/s41598-025-03237-8

27. K. K. Ahmed, M. Ozisik, H. Emadifar, Optical soliton solutions and stability analysis of the stochastic perturbed quintic DNLSIII model, *Results Eng.*, **28** (2025), 107185. https://doi.org/10.1016/j.rineng.2025.107185

28. M. S. Iqbal, A. R. Seadawy, M. Z. Baber, M. W. Yasin, N. Ahmed, Solution of stochastic Allen-Cahn equation in the framework of soliton theoretical approach, *Int. J. Mod. Phys. B*, **37** (2023), 2350051. https://doi.org/10.1142/S0217979223500510

29. L. Akinyemi, M. Şenol, M. S. Osman, Analytical and approximate solutions of nonlinear Schrödinger equation with higher dimension in the anomalous dispersion regime, *J. Ocean Eng. Sci.*, **7** (2022), 143–154. https://doi.org/10.1016/j.joes.2021.07.006

30. Z. Yan, Z. Pan, G. Hu, H. Yan, Finite-time annular domain guaranteed cost control for uncertain mean-field stochastic systems with Wiener and Poisson noises, *IEEE T. Syst. Man Cy.: Syst.*, **55** (2025), 7981–7993. https://doi.org/10.1109/TSMC.2025.3598993

31. S. Kumar, S. K. Dhiman, Exploring cone-shaped solitons, breather, and lump-forms solutions using the lie symmetry method and unified approach to a coupled breaking soliton model, *Phys. Scr.*, **99** (2024), 025243. https://doi.org/10.1088/1402-4896/ad1d9e

32. S. Shagolshem, B. Bira, K. V. Nagaraja, Analysis of soliton wave structure for coupled Higgs equation via Lie symmetry, Paul Painlevé approach and the unified method, *Nonlinear Dyn.*, **113** (2025), 11999–12020. https://doi.org/10.1007/s11071-024-10697-6

33. R. Ur Rahman, W. A. Faridi, M. A. El-Rahman, A. Taishiyeva, R. Myrzakulov, E. A. Az-Zo'bi, The sensitive visualization and generalized fractional solitons' construction for regularized long-wave governing model, *Fractal Fract.*, **7** (2023), 136. https://doi.org/10.3390/fractalfract7020136

34. R. Ur Rahman, Z. Hammouch, A. S. A. Alsubaie, K. H. Mahmoud, A. Alshehri, E. A. Az-Zo'bi, et al., Dynamical behavior of fractional nonlinear dispersive equation in Murnaghan's rod materials, *Results Phys.*, **56** (2024), 107207. https://doi.org/10.1016/j.rinp.2023.107207

35. M. S. Ullah, M. Z. Ali, H. O. Roshid, Bifurcation, chaos, and stability analysis to the second fractional WBBM model, *PlOS One*, **19** (2024), e0307565. https://doi.org/10.1371/journal.pone.0307565

36. S. Barik, S. Behera, Soliton solutions with stability, bifurcation analysis and phase portraits of Kudryashov-Sinelshchikov equation, *Chaos Soliton. Fract.*, **201** (2025), 117367. https://doi.org/10.1016/j.chaos.2025.117367

37. N. Alessa, S. M. Boulaaras, M. H. Rasheed, H. Ur Rehman, Bifurcation analysis, phase portraits and optical soliton solutions of the perturbed temporal evolution equation in optical fibers, *Mod. Phys. Lett. B*, **39** (2025), 2550047. https://doi.org/10.1142/S0217984925500472

38. M. A. S. Murad, W. A. Faridi, A. Jhangeer, M. Iqbal, A. H. Arnous, F. Tchier, The fractional soliton solutions and dynamical investigation for planer Hamiltonian system of Fokas model in optical fiber, *Alex. Eng. J.*, **121** (2025), 27–37. https://doi.org/10.1016/j.aej.2025.02.052

39. M. A. S. Murad, A. H. Arnous, W. A. Faridi, M. Iqbal, K. S. Nisar, S. Kumar, Two distinct algorithms for conformable time-fractional nonlinear Schrödinger equations with Kudryashov's generalized non-local nonlinearity and arbitrary refractive index, *Opt. Quant. Electron.*, **56** (2024), 1320. https://doi.org/10.1007/s11082-024-07223-8

40. Y. He, M. Yuan, Q. Li, L. Tang, W. Yang, Y. Ping, et al., Feasibility study of mechanical stress wave detection in power semiconductor devices using bare FBG sensors, *IEEE Sens. J.*, **25** (2025), 39849–39857. https://doi.org/10.1109/JSEN.2025.3615108

AIMS Press